Available online at www.sciencedirect.com
SCIENCE DIRECT®
International Journal of Heat and Mass Transfer 49 (2006) 1274–1286
International Journal of HEAT and MASS TRANSFER
www.elsevier.com/locate/ijhmt

A comparative study on showerhead cooling performance

C. Falcoz [a], B. Weigand [b,*], P. Ott [a]

[a] Ecole Polytechnique Fédérale de Lausanne (EPFL), Laboratoire de Thermique Appliquée et de Turbomachines (LTT), 1015 Lausanne, Switzerland
[b] Institut für Thermodynamik der Luft- und Raumfahrt (ITLR), Stuttgart University, Pfaffenwaldring 31, 70569 Stuttgart, Germany

Received 15 December 2004; received in revised form 31 August 2005
Available online 6 December 2005

Abstract

In modern gas turbines, the turbine airfoil leading edge is currently protected from the hot gas by specific film cooling schemes, so called showerhead cooling. The present paper shows a numerical study of different showerhead cooling geometries. The 3D finite element program ABAQUS as well as a 2D finite element program have been employed to predict the showerhead cooling performance. In the numerical calculations, the different cooling effects and their contribution to the total showerhead cooling performance have been investigated separately. From the numerical calculations a simple method has been derived which enables the prediction of the performance of a 3D showerhead cooling scheme by simple 2D computations. Experimental investigations on showerhead cooling have been presented in a companion paper [C. Falcoz, B. Weigand, P. Ott, Experimental investigations on showerhead cooling on a blunt body. Int. J. Heat Mass Transfer, in press].

1. Introduction

In modern gas turbine designs, there is a strong desire to increase the inlet hot gas temperature of the turbine. This would lead to much higher blade temperatures than the maximum allowable metal temperature. In order to protect the turbine blades from melting, extensive cooling by internal air flow is needed. Usually a combination of internal convective cooling and external film cooling is employed. The cooling designs of these parts have to be highly efficient, because of the fact that a larger cooling mass flow rate degrades the thermal efficiency of the thermodynamic cycle of the gas turbine. This is especially true for the application of film cooling, where a protective film of cold air is spread around the blade and large cooling mass flows are required. Because of the importance of film cooling for turbine blade design, the subject has been studied extensively and a large part of the results are available in the open literature. Several review articles on film cooling are published on this subject. A summary of several papers concerning film cooling can be found in [1,8]. Showerhead cooling is used in order to protect the stagnation point area against the extremely high gas temperatures. In contrast to film cooling on a turbine blade, the coolant flow out of the holes in the nose of the profile can hardly form a good cooling film around the profile. On the other side, the coolant flow takes heat from the blade material while passing through the relatively long coolant holes in the nose of the profile. To extend the coolant holes in length, mostly these holes are radially inclined. Because of the above cited features of showerhead cooling, the cooling of the nose of an airfoil by showerhead cooling contents the external film cooling, the internal cooling in the coolant holes as well as the cooling inside the main coolant channel inside the blade. In order to evaluate the performance of showerhead cooling schemes, all three aspects of showerhead cooling have to be addressed. This is the aim of the present paper. The paper shows the evaluation of the global performance of the showerhead cooling model by using 2D and 3D Finite Element Models (FEM).

In an early study, Mayle and Camarata [2] investigated multihole aircraft turbine blade cooling. This particular

* Corresponding author. Tel.: +49 711 685 3590; fax: +49 711 685 2317.
E-mail address: bw@itlr.uni-stuttgart.de (B. Weigand).

0017-9310/$ - see front matter © 2005 Elsevier Ltd. All rights reserved.
doi:10.1016/j.ijheatmasstransfer.2005.10.013

Nomenclature

A	area [m^2]
c_p	specific heat at constant pressure [J/(kg K)]
D	leading edge cylinder diameter [m]
d	cooling hole diameter [m]
DR	coolant-to-mainstream density ratio, $DR = \rho_c/\rho_g$ [–]
G	blowing ratio, $G = \rho_c u_c/\rho_g u_\infty$, referred to hole entrance [–]
h	heat transfer coefficient [W/(m^2 K)]
I	momentum flux ratio, $I = \rho_c u_c^2/\rho_g u_\infty^2$, referred to hole entrance [–]
k	thermal conductivity [W/(m K)]
L	hole length [m]
M	approach Mach number, $M = u_\infty/a, a = \sqrt{\kappa RT}$ [–]
$\dot{m}$	mass flow [kg/s]
Nu	Nusselt number, $Nu = hD/k$ [–]
p	pitch or spanwise spacing between holes in one row [m]
q	surface heat flux [W/m^2]
Re_D	Reynolds number, $Re_D = \rho_g u_\infty D/\mu$ [–]
Re_d	Reynolds number in the cooling hole, $Re_d = \rho_c u_c d/\mu$ [–]
T	temperature [°C], [K]
Tu	free-stream turbulence intensity [%]
u	velocity [m/s]
u_∞	approach velocity to model [m/s]
x, y, z	cartesian coordinates [m]

Greek symbols

β	spanwise inclination angle to surface [°]
ε	cooling effectiveness, $\varepsilon = (T_{rg} - \widetilde{T}_m)/(T_{tg} - T_c)$ [–]
γ	row exit location angle measured from stagnation line [°]
η	film cooling effectiveness, $\eta = (T_{aw} - T_{rg})/(T_{tc} - T_{tg})$ [–]
φ	streamwise inclination angle [°]
μ	dynamic viscosity [N s/m^2]
ρ	density [kg/m^3]
Γ	contour [m]
Ω	surface [m^2]

Subscripts

c	coolant
f	with film cooling
g	hot gas
r	recovery conditions
t	total conditions
w, aw	wall, adiabatic wall

type of cooling scheme relies on the convective cooling inside the holes as well as on the protective film. The authors showed that an increase in film cooling effectiveness had a greater benefit at lower blowing rates than at higher ones. Kasagi et al. [3] presented a numerical prediction scheme for the calculation of the temperature distribution inside a full-coverage film-cooled (FCFC) wall. The heat transfer characteristics were discussed considering the heat balance of a unit hole element. The variation of the solid wall temperature was neglected over the plate thickness. The results showed that the thermal properties had a significant influence on the overall cooling effectiveness due to the heat conduction inside the wall. Kumada et al. [4] measured the local heat transfer coefficients on a brass FCFC plate. The local Stanton numbers were successfully measured on both film-cooled and backside surfaces, but the limitation of the experimental apparatus did not allow for measurements on the inside surface of the holes. Nevertheless, the authors suggested the importance of the convective cooling inside the holes as compared to the backside surface and concluded that improving heat transfer characteristics on the backside surface would appreciably increase the overall cooling effectiveness. In a more recent paper, Wadia and Nealy [5] proposed an engineering design model that treated the gas-to-surface heat transfer coefficient with film cooling, including the active heat transfer within and upstream of the film hole array. The predictive model was derived on a cylindrical showerhead model. The capabilities of the analytical model were explored for typical high temperature first stage turbine vanes and rotor blades. The values predicted for the overall cooling effectiveness were validated with temperature measurements performed on stainless steel cylindrical models. The authors concluded that the active cooling mechanisms within and upstream of the film hole array produced the principal beneficial effects of showerhead cooling. Martiny et al. [6] focused on modeling the enthalpy rise of the coolant along the hole axis. The authors presented a mathematical model for the calculation of the wall temperatures of an effusion-cooled plate. The heat transfer coefficient was assumed to be constant along the hole axis. The model was validated with experimentally determined coolant outlet temperatures. A parametric study was conducted in order to show the influence of the individual cooling contributions on the overall cooling effectiveness. A reference solution was defined for constant geometrical parameters, as well as specific mainstream and coolant flow conditions. Martiny et al. [6] concluded that the most important part of the incoming heat flux was absorbed by the coolant as it passed through the holes. From the above given literature review it can be seen that a rigorous analysis of the showerhead

cooling by 3D and 2D methods is still missing. This is one of the aims of the present study.

2. Investigated models and cases

For the present numerical calculations, different models for showerhead cooling have been investigated. These models consist of cylindrical models and a blunt body. Both model types have different showerhead cooling geometries.

2.1. Cylinder models

The showerhead cooling geometries for the cylinders consist of a four- and a three-row configuration in a staggered arrangement. Cylindrical holes of 0.9 mm diameter, which have a spanwise injection angle of $\beta = 45°$ and a streamwise inclination angle of $\varphi = 90°$, were chosen. Rows are distributed symmetrically with respect to the stagnation point. Fig. 1 gives an overview of the geometries. The coolant, which is provided from a single plenum chamber, comes from the bottom. The different geometrical parameters are listed in Table 1. Experiments for the external cooling were performed by Hoffs et al. in a free jet facility [7]. They measured the external heat transfer and the adiabatic film cooling effectiveness on the cylinders. The approach Mach number for these tests was about $M = 0.3$. The tests were performed for the nominal angle of attack of 0°. The turbulence level was Tu = 7% (see also [7]).

Table 1
Geometrical parameters describing the showerhead configurations for the cylindrical model

		Four-row configuration	Three-row configuration
Number of rows		4	3
Diameter ratio	d/D	0.03	0.03
Exit location angles [°]	γ	$-21/-7/+7/+21$	$-21/0/+21$
Spanwise pitch	p/d	5.0	6.3
Hole length	L/d	4.7	4.7
Streamwise inclination angle [°]	φ	90	90
Spanwise inclination angle [°]	β	45	45
Exit shape		Cylindrical	Cylindrical

2.2. Blunt body model

Experiments on a blunt body geometry have been performed by Falcoz (see [1,8]) in a linear cascade test facility. The geometry of the blunt body and the here investigated cooling hole geometries are depicted in Fig. 2. The film hole injection geometries of the blunt bodies are designed for a turbine blade/vane leading edge. Fig. 2 shows the different showerhead configurations. The coolant, which is provided from a single plenum chamber, comes from the bottom. Showerhead geometry SHG1 consists of four staggered rows of cylindrical holes with a diameter of 0.7 mm. Rows are placed symmetrically around the stagnation line. A modern configuration of fan-shaped holes was considered in addition to classical cylindrical holes. Configuration SHG2 uses the same cooling arrangement in terms of hole diameter, row number, hole spacing, and inclination angles, but with modified hole exits. SHG2 illustrates a conical portion with a 1.8° open angle creating a diffuser of four hole diameters deep. The effective surface area of the hole exits is increased by a factor of 1.5 compared to the cylindrical holes. All geometrical parameters are summarized in Table 2. The tests were performed for 0° incidence and for approach Mach numbers of $0.14 < M < 0.36$ ($0.58\text{E}+05 < Re_D < 1.52\text{E}+05$). The turbulence level was Tu = 10% and the density ratio DR was between 1.15 and 1.18. Experimental results of the film cooling performance are reported in [1,8].

2.3. Investigated cases

The purpose of the present numerical study was to evaluate the combined effects of external cooling (due to film cooling), heat conduction and internal convection cooling (through the holes and inside the plenum chamber) on

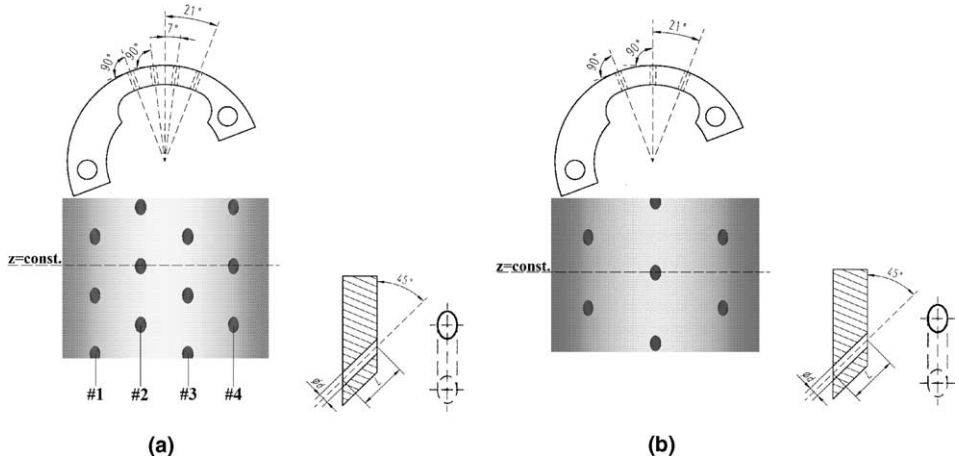

Fig. 1. Showerhead geometries for the cylinder models. (a) Four row configuration and (b) three row configuration.

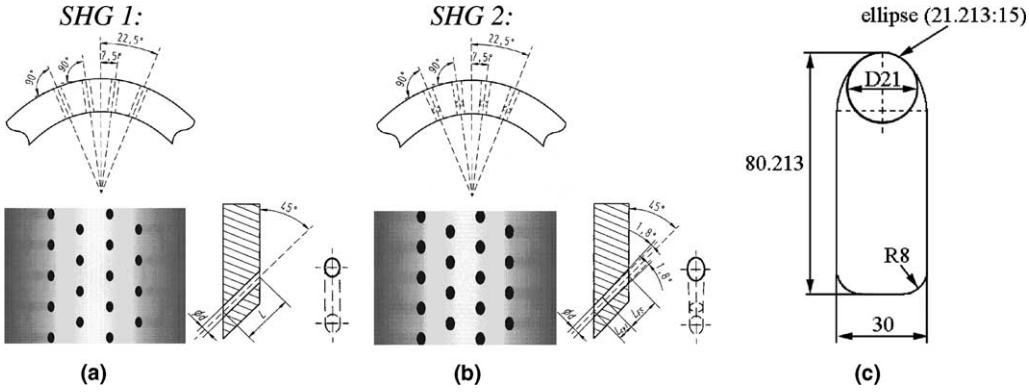

Fig. 2. Geometrical data of the blunt body geometry (dimensions in [mm]) and the film cooling configurations. (a) Cylindrical holes, (b) Conical holes and (c) Blunt body.

Table 2
Geometrical parameters describing the showerhead configurations for the blunt body

		SHG1	SHG2
Diameter ratio	d/D	0.033	0.033
Exit location angles [°]	γ	±22.5/±7.5	±22.5/±7.5
Spanwise pitch	p/d	4	4
Hole length	L/d	6	6
Streamwise inclination angle [°]	φ	90	90
Spanwise inclination angle [°]	β	45	45
Area ratio		1	1.5
Exit shape		Cylindrical	Conical

Table 3
Temperature dependent thermal conductivity of a gas turbine blade alloy

Temperature [K]	Thermal conductivity, k [W/(m K)]
373.15	9.6
473.15	11.0
573.15	12.4
673.15	13.9
773.15	15.3
873.15	16.9
973.15	18.4
1073.15	20.0
1173.15	21.4
1273.15	23.0

the material temperature. In order to analyze and interpret these effects, computations were performed for different showerhead cooling models by varying several parameters (main flow conditions, blowing ratio, level of cooling inside the plenum chamber, ...). Therefore, several sets of numerical calculation conditions were developed. Two main groups can be distinguished:

1. EPFL conditions (test conditions), where the calculation conditions were evaluated for Plexiglas models tested at low temperature. This test case has a very low heat conductivity in the material (Plexiglas, $k = 0.19$ W/(m K)). Therefore, the backside cooling (plenum) effect is nearly decoupled from the external film cooling.
2. REC (real engine conditions), where the calculation conditions were estimated for a gas turbine airfoil alloy exposed to a high-pressure and high-temperature environment. For this case, backside cooling (plenum) and film cooling are strongly linked by heat conduction in the blade material. In addition a large amount of heat is transferred to the coolant flowing in the film holes. The temperature dependent thermal conductivity of the material is given in Table 3.

Appendix A and [8] give an overview on how the individual boundary conditions for the calculations have been derived from experimental data and correlations.

3. Numerical calculations

The aim of the present study was the evaluation of the different cooling mechanisms for showerhead cooling schemes. As mentioned above, the external heat transfer has been measured on cylinder and blunt body models. This provides the external boundary conditions for the finite element analysis described in the present chapter (see also Appendix A). In order to evaluate the effects of varying the showerhead cooling scheme of turbine vanes or blades in a real engine, the material temperature field needs to be predicted. The governing equation, namely the differential equation of heat conduction, was solved using 3D and 2D finite element programs. For the case of an isotropic body with temperature dependent thermal conductivity and with heat sources, this equation can be expressed as (Carslaw and Jaeger [9]):

$$\frac{\partial}{\partial x}\left(k\frac{\partial T}{\partial x}\right)+\frac{\partial}{\partial y}\left(k\frac{\partial T}{\partial y}\right)+\frac{\partial}{\partial z}\left(k\frac{\partial T}{\partial z}\right)+\dot{q}_{\mathrm{i}}=0 \tag{1}$$

3.1. Finite element calculations (3D) with ABAQUS

Different 3D finite element calculations have been carried out by using the commercial program ABAQUS [10]. Eq. (1) describes an elliptic problem that allows different boundary conditions, to be specified. For the present

numerical simulations, boundary conditions of the third kind have been applied:

- at the external surface exposed to the main stream (Ω_g) heat is transferred by convection to the surface:

$$-k\frac{\partial T}{\partial n}\bigg|_w = h_f(T_{aw} - T_w) \tag{2}$$

- in the plenum, the surfaces exchange heat by convection with the coolant (Ω_{plen}):

$$-k\frac{\partial T}{\partial n}\bigg|_w = h_{c,plen}(T_{c,plen} - T_w) \tag{3}$$

- at the cooling hole surfaces (Ω_h) heat is exchanged by convection with the coolant:

$$-k\frac{\partial T}{\partial n}\bigg|_w = h_{c,hole}(T_{c,hole} - T_w) \tag{4}$$

where $\partial/\partial n$ denotes differentiation along the outward-pointing vector normal to the surface Ω. In addition, the simulations are done on an extracted part of the model in order to reduce the computational time. Therefore, periodic boundary conditions are applied to the upper (Ω_{UP}) and lower (Ω_{DOWN}) surfaces that delimit the sub-model:

$$T(x,y,z = z_{UP})|_{\Omega_{UP}} = T(x,y,z = z_{DOWN})|_{\Omega_{DOWN}} \tag{5}$$

The heat sources in Eq. (1) have been set to zero for the 3D calculations. The geometrical model is first designed with the CAD-program I-DEAS 7 [11]. A periodic part of this geometry is selected for the solid mesh generation. The automated mesh generation algorithm included in I-DEAS is used to realize the discretization of the computational domain. Typical meshes for the cylinder model are depicted in Fig. 3. Extensive grid sensitivity studies have been done for the 3D calculations with ABAQUS. For example, three different meshes were carried out for the four-row cylindrical model. The calculations were performed at engine-like conditions for two blowing rates, as well as for different backside heat transfer coefficients. The influence of the mesh refinement on the mean solid temperature is shown in Table 4. The sensitivity analysis showed that the mesh heterogeneity had only a very weak influence on the mean solid temperature. Due to the large number of elements/nodes defining the finest mesh (#1) and the high execution time required for this grid, the intermediate mesh (#2) was preferred for the 3D simulations. In fact, this mesh offered a very good compromise between the accuracy of the predicted temperatures and the calculation time needed to compute the temperature field.

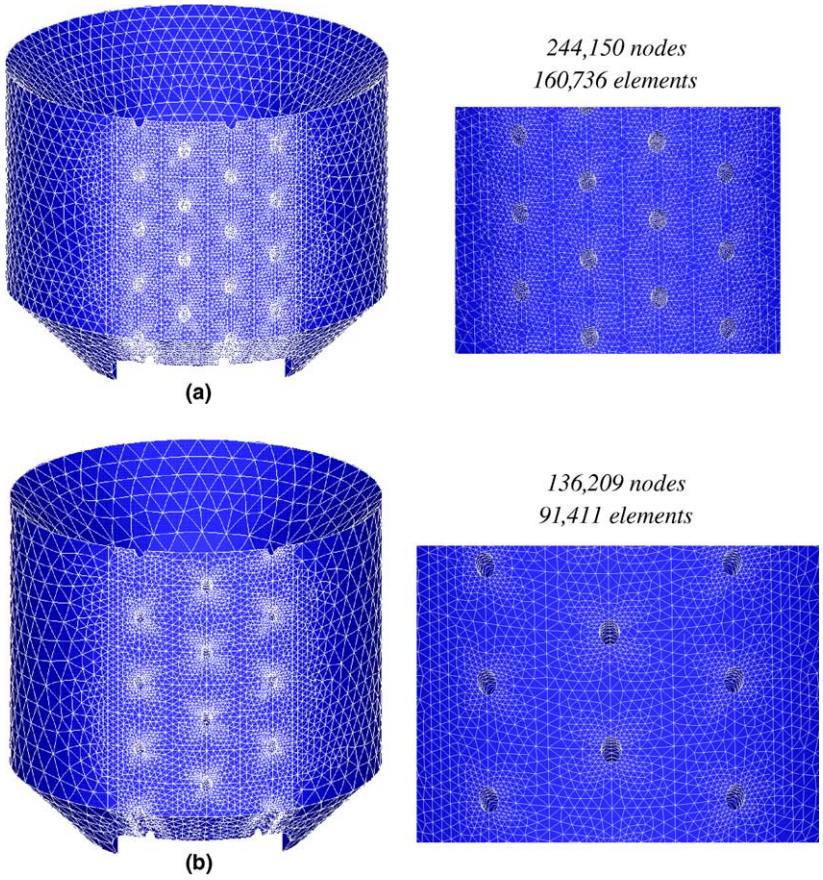

Fig. 3. 3D meshes for the four row configuration on the cylinder. (a) Fine mesh of the computational domain for the four row configuration and (b) mesh for the three hole configuration.

Table 4
Influence on the mesh refinement on the mean solid temperature for different 3D ABAQUS calculations

G	h_{plen} [W/(m^2 K)]	Mean solid temperature [°C]		
		Mesh #1 244,150 nodes 160,736 elements	Mesh #2 122,250 nodes 78,642 elements	Mesh #3 78,249 nodes 49,291 elements
0.44	150	1179.12	**1179.07**	1178.99
0.44	380	1131.96	**1131.92**	1131.83
1.81	440	1091.87	**1091.89**	1091.94
1.81	1100	1000.12	**1000.17**	1000.17

3.2. Finite element calculations (2D) with a 2D heat conduction solver (2DHCS)

2DHCS is a program-package that consists of a grid generator, a 2D heat conduction solver, and a graphical postprocessor. This finite element program, developed by ALSTOM-Power Switzerland, is usually used for the 2D heat conduction analysis for blade profiles with arbitrary internal cooling channels and film cooling holes. In the present work, this software was employed to evaluate the temperature distribution for several showerhead-cooled configurations. The main difference between ABAQUS and 2DHCS consists in the way the cooling holes are taken into account in the calculations. In 2DHCS, the cooling holes are modeled by using heat sinks in the material, assuming that they absorb an equivalent heat flux as the film cooling holes. As a result, for a 2D homogeneous isotropic solid, whose thermal conductivity is temperature-dependent, and for a steady-state temperature distribution, the heat conduction equation is simplified from Eq. (1) to

$$\frac{\partial}{\partial x}\left(k\frac{\partial T}{\partial x}\right)+\frac{\partial}{\partial y}\left(k\frac{\partial T}{\partial y}\right)+\dot{q}_i=0 \tag{6}$$

Before Eq. (6) can be solved, it is necessary to express the boundary conditions. Boundary conditions of the third kind are used:

- on the external contour exposed to the main stream (Γ_g):

$$-k\frac{\partial T}{\partial n}\bigg|_w=h_f(T_{aw}-T_w) \tag{7}$$

- on the internal contour describing the plenum chamber (Γ_{plen}):

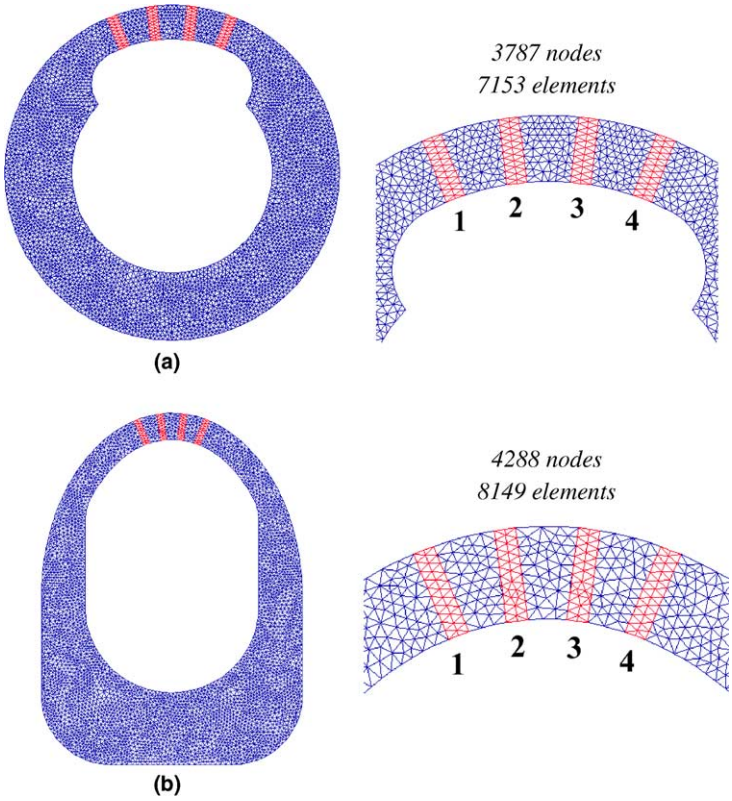

Fig. 4. 2D meshes for the four row configuration on the cylinder and on the blunt body. (a) 2D mesh of the computational domain (four rows—cylinder) and (b) 2D mesh of the computational domain (four rows—blunt body).

$$-k\left.\frac{\partial T}{\partial n}\right|_{w} = h_{c,plen}(T_{c,plen} - T_w) \tag{8}$$

where $\partial/\partial n$ denotes the normal derivative along the boundary Γ of the domain. With respect to the cooling holes, heat sink temperatures and heat transfer coefficients are prescribed along the hole axis in order to evaluate an equivalent heat flux. The 2D calculations are performed on a particular cut of the model used for the 3D simulations. The internal and external contours of the 2D geometries are defined with discrete points. The spatial discretization of the 2D domain is a completely automated process. Here, the grid generation is based on a Delaunay algorithm, described in [12]. Typical meshes are depicted in Fig. 4 for the cylindrical model and for the blunt body. Grid independency studies for the 2D calculations have been done extensively. Typically around 3500 nodes and 7000 elements where found to be sufficient.

4. Numerical results

Commonly, the cooling performance of a showerhead-cooled configuration can be characterized in terms of the overall cooling effectiveness. The overall cooling effectiveness corresponds to a non-dimensional form of the material temperature. Hence, the latter, noted as ε, is chosen as the parameter and is defined by

$$\varepsilon = \frac{T_{rg} - \widetilde{T}_m}{T_{tg} - T_{tc}} \tag{9}$$

where T_{rg} is the recovery temperature of the hot gas, $\widetilde{T}_m$ is the average metal temperature and T_{tc} is the total temperature of the coolant at the entrance of the holes. The above averaged metal temperature has been defined by

$$\widetilde{T}_m = \frac{1}{V_{total}} \sum_{j=1}^{M} \widetilde{T}_j V_j \quad \text{for a 3D geometry (ABAQUS)}$$
$$\widetilde{T}_m = \frac{1}{A_{total}} \sum_{j=1}^{M} \widetilde{T}_j A_j \quad \text{for a 2D geometry (2DHCS)} \tag{10}$$

where $\widetilde{T}_j$ are the average temperature of each element, V_j, A_j are the volume or the area of each element and M indicates the total number of elements.

4.1. Numerical results for the cylindrical models

The twofold aim of these simulations is to identify the different cooling mechanisms present in a film-cooled model and to compare the capabilities of both 3D and 2D finite element programs to evaluate the cooling performance of this film-cooled configuration. Numerical simulations are mostly performed at real engine conditions for a real blade alloy (referred to as REC), but additional calculations are also done at experimental conditions on a low-conductivity material (referred to as EPFL conditions).

4.1.1. Four row configuration

We will start our considerations with the study of the influence of the blowing ratio on the material temperature. The three cooling mechanisms present in the problem were included in the numerical simulations. Computations were performed at REC for four blowing ratios combined with two levels of backside cooling (plenum). All showerhead configurations have a unique plenum chamber to feed the rows of cooling holes. Therefore, the blowing ratio G refers to a global quantity, defined as

$$G = \frac{\rho_c u_c}{\rho_g u_g} = \frac{\dot{m}_c}{A_{c,tot}} \frac{1}{\rho_g u_g} \tag{11}$$

where $\dot{m}_c$ is the mass flow of the coolant provided to the plenum chamber and $A_{c,tot}$ represents the overall surface of the cooling holes. Typical material temperature distributions calculated with ABAQUS are depicted in Fig. 5. In order to facilitate the comparison, identical scaling is used for both blowing ratios. The comparison shows that the outer surface temperature is lower at higher blowing ratios. The 3D material temperature distributions give qualitative information, but they do not allow definitive conclusions with regards to the influence of the blowing ratio. Therefore, the overall cooling effectiveness, defined by Eq. (9),

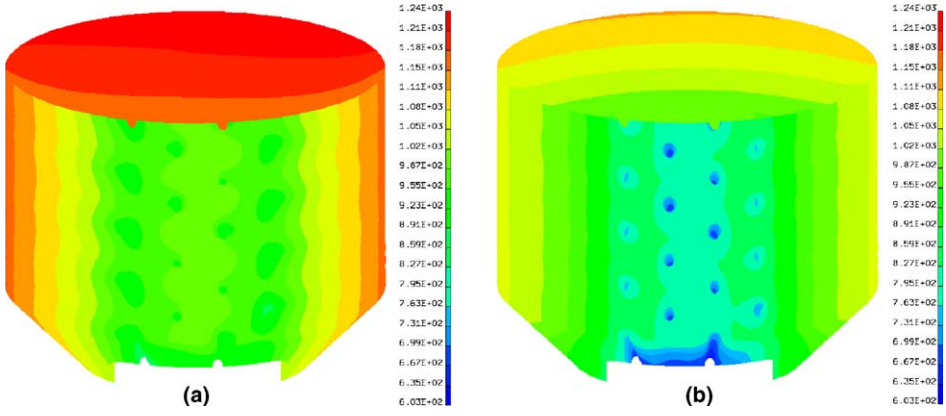

Fig. 5. 3D material temperature distribution calculated for the four row cylinder at REC for two blowing rates ($G = 0.44, 1.81$). (a) $G = 0.44$, $h_{plen} = 380$ W/(m^2 K), $\tilde{T}_m = 1131.92$ °C and (b) $G = 1.81$, $h_{plen} = 1100$ W/(m^2 K), $\tilde{T}_m = 1000.17$ °C.

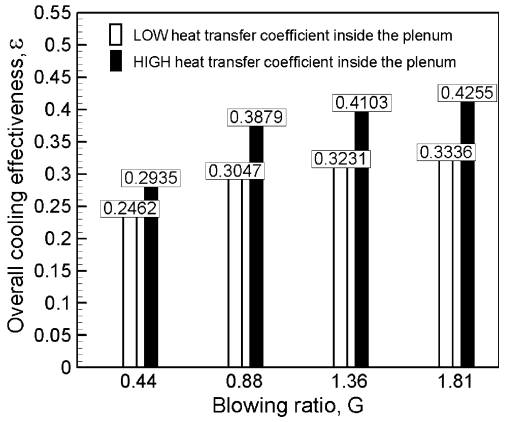

Fig. 6. Influence of the blowing ratio at REC: Results obtained with ABAQUS for the four row cylinder configuration.

was calculated for all test conditions. The results are shown in Fig. 6. For a constant level of backside cooling (plenum), either at low or high h_{plen}, the overall cooling effectiveness increases with increasing blowing ratio. For the same blowing ratio, the overall cooling effectiveness is higher if the backside cooling is greater, which means: the more coolant injected, the lower the mean solid temperature. Since all the cooling mechanisms described before are strongly coupled in a real film-cooled situation, their individual contributions to the showerhead cooling performance were investigated. "Switching on and off" the heat transfer coefficients inside the holes and on the cold side, and the film cooling effectiveness on the hot gas side, the contributions of the different cooling mechanisms can be evaluated. In varying these parameters independently, one must keep in mind that in a real situation the variation of one parameter will always affect all the others. To discuss the influence of the different cooling mechanisms on the overall cooling effectiveness, a fictitious reference solution—also called the ideal case—was defined. For this ideal case, the temperature distribution is evaluated in the material by taking into account the three cooling mechanisms and assuming that the enhancement of the external heat transfer coefficient due to the presence of the film and the cooling holes is negligible. Therefore, the heat transfer coefficient applied on the hot gas side is the one corresponding to the case without blowing. On the whole, the ideal case corresponds to the highest overall cooling effectiveness that can be achieved with a specific showerhead cooling configuration. Since the blowing rates and the backside heat transfer coefficients vary in the current study, the ideal overall cooling effectiveness is not a constant value characterizing all cases. The effects of the three different cooling mechanisms—taken individually or in pairs—were studied at REC. Referring to Fig. 7, the overall cooling effectiveness calculated for the ideal case is 14–17% higher than that of the original case. This conclusion clearly demonstrates the side

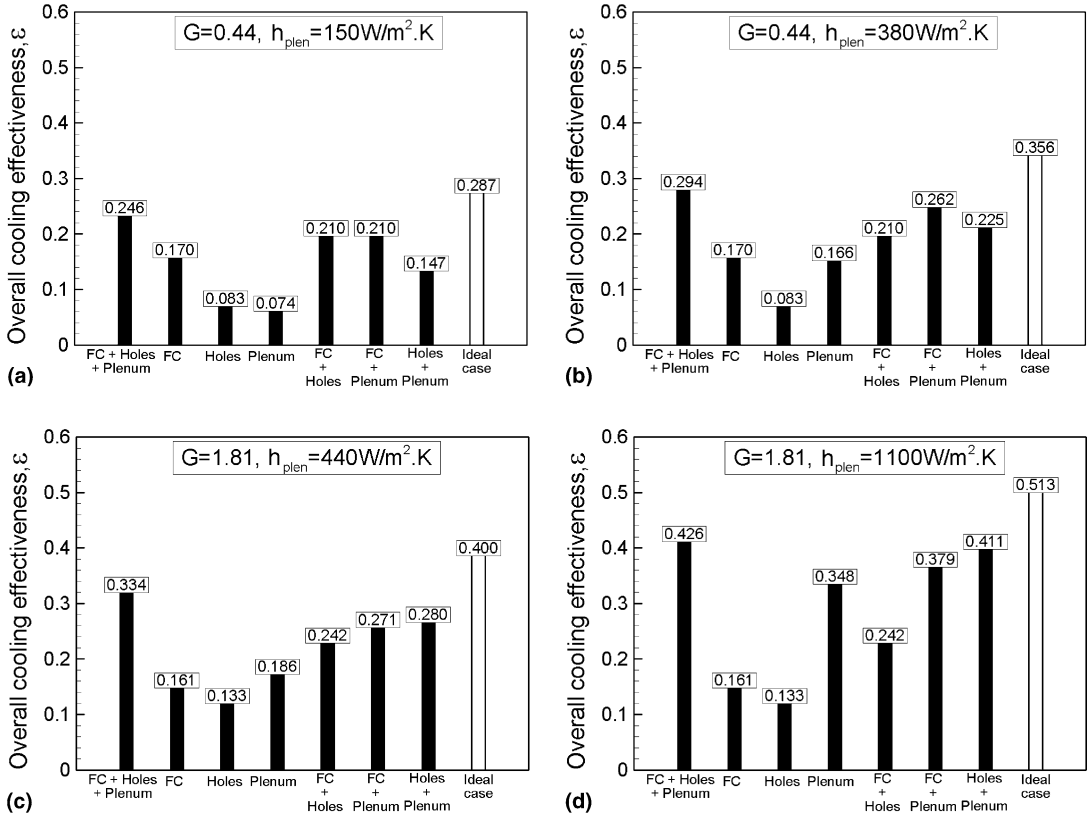

Fig. 7. Contributions of the different cooling mechanisms at REC: ABAQUS calculations for the four row cylinder configuration. (a) Low G, low h_{plen}, (b) low G, high h_{plen}, (c) high G, low h_{plen}, (d) high G, high h_{plen}.

effects of the presence of the film and the cooling holes. In fact, in a showerhead, the hot gas side heat transfer coefficient is enhanced due to the presence of the injected coolant and the film holes that both disturb the boundary layer, leading locally to an increased turbulence level [1]. The external film cooling effect (referred to as FC in Fig.7) is more pronounced at low blowing ratios, leading to a higher overall cooling effectiveness. In a previous experimental study, Hoffs et al. [7] investigated the influence of the blowing ratio on the film cooling effectiveness for the same showerhead-cooled model. He reported that $G = 0.44$ offered the highest film cooling effectiveness, but also high heat transfer coefficients. He found lower values of the film cooling effectiveness for $G = 1.81$. In conclusion, the blowing ratio that offers the highest film cooling effectiveness provides the highest overall cooling effectiveness when only the contribution of the external film cooling is considered for the numerical simulations. With regards to the cooling holes contribution, the higher the blowing ratio, the higher the overall cooling effectiveness. This is a direct consequence of the heat flux absorbed by the flow passing through the holes at high blowing ratio. In fact, lower coolant velocities in the holes cause lower heat transfer coefficients, hence a lower heat absorption. With an increasing backside heat transfer coefficient for a constant blowing ratio, the portion of the heat removed inside the holes (with respect to the ideal case) decreases from 29% to 23% at $G = 0.44$ and from 33% to 26% at $G = 1.81$. With regards to the backside cooling (coolant plenum), for a constant blowing ratio, the overall cooling effectiveness increases dramatically with increasing values of h_{plen}. The backside cooling represents an important potential to reduce the material temperature, hence the necessity to develop efficient internal cooling methods for turbine blades, such as impingement, ribs and pin fins. On the whole, the internal convective cooling, including both cooling effects generated inside the cooling holes and on the cold side, depends strongly on the blowing ratio and the heat transfer coefficient inside the plenum chamber. At low G, the internal convective cooling absorbs 51–63% of the heat. At high G, the internal convective cooling absorbs 70–80% of the heat. In all cases, most of the heat is removed from the material by the internal convective cooling.

It would be of great interest if the before mentioned 3D processes in the showerhead area could accurately be predicted by a simple 2D program. In order to explore this opportunity, several 2D calculations have been done for the four row configuration. Starting with the simplest approach, a 90° cut ($z = \text{const.}$, see Fig. 1) can be made through the cylinder and the plane extracted can be analyzed by a 2D finite element solver. For this approach, it has been assumed that all four rows of cooling holes lay in the same 2D cut. They are modeled by heat sinks in the material area, where the holes are present. Comparing the overall effectiveness obtained from the 2D calculations with the ones from the 3D calculations shows some discrepancies (see Fig. 8). For all cases, the 2D calculations lead to a much higher overall cooling effectiveness, although the enhancement remains moderate for the low-conductivity case. Referring to Fig. 8 the differences between the 2D and 3D results are almost constant over all blowing ratios, except at $G = 0.44$. It seems that the 2D calculations take into account an additional phenomenon that induces a supplementary material temperature reduction, leading to higher values of ε. In fact, for the 2D simulations presented above, the four rows of cooling holes were assumed to be in the same plane, whereas the rows were staggered in the 3D simulations. Hence, the heat removed from the solid increased for the 2D calculations, especially for a high conductivity material. In order to test the influence of the number of rows, additional simulations—referred as quasi-3D calculations—were performed. They consist of performing two sets of 2D simulations considering two rows out of four (rows #1 and #3 and rows #2 and #4). The overall cooling effectiveness corresponding to the quasi-3D calculation is defined by the arithmetic mean of the two values of the mean metal temperature $\widetilde{T}_{\text{m}}$ obtained for each case. Therefore, the side

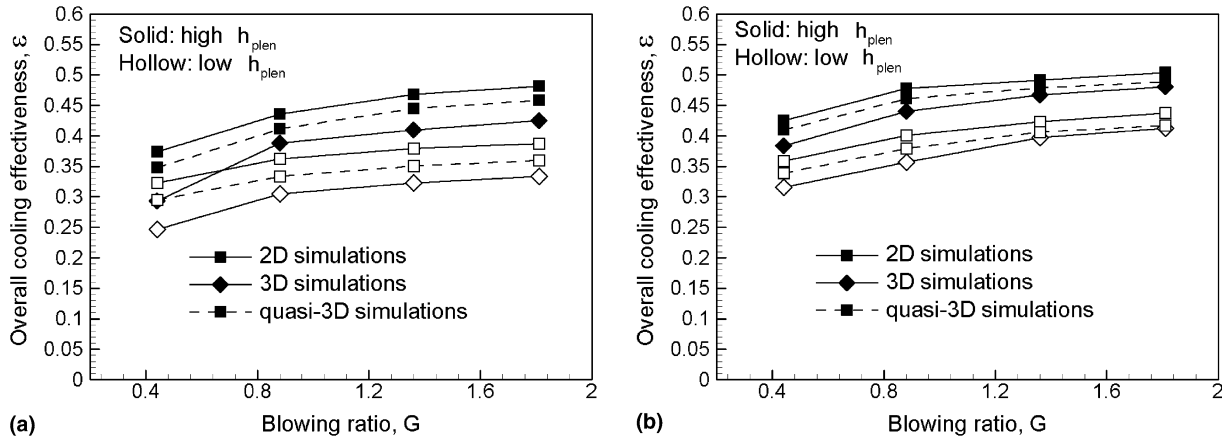

Fig. 8. Comparisons between the 3D, 2D, and quasi-3D simulations corresponding to the four row cylindrical model. (a) Real blade material (REC) and (b) low-conductivity material (EPFL conditions).

effect of considering all rows at the same time should be eliminated. With regard to Fig. 8 the quasi-3D simulations seem to be a valuable approach to reduce drastically the discrepancies between the 3D and 2D numerical results. On the whole, the deviations between the quasi-3D and 3D calculations are twice as small as those between the 2D and 3D calculations. Although the quasi-3D simulations allow a better fitting of the 3D results, there nevertheless remains a small deviation between the quasi-3D and the 3D results. Yet another explanation can be considered. In fact, both 2D and quasi-3D simulations were performed on a 90°-cut of the four-row cylindrical model, whereas the cooling holes have a 45°-inclination angle from the surface in the 3D geometry. Therefore, additional simulations (both 2D and quasi-3D) were done on a 45°-cut of the four-row cylinder. The advantage of performing simulations on a 45°-cut of the model is to take into account the same hole length as the one considered in the 3D simulations. Hence, the heat transfer coefficient and coolant temperature distributions along the cooling hole centerline are identical in the 3D model and its 45°-cut. The heat removed from the cooling holes is then equivalent in both cases provided that the wall temperature distribution is equal. Fig. 9 shows some comparisons between the 3D and the quasi-3D calculations. This means that two 45° cuts with either two cooling holes have been run in 2D and the results have been combined as described before. As it can be seen, the agreement is very good. This shows nicely, how a 2D program can be used in order to accurately predict the 3D showerhead cooling performance.

4.1.2. Three row configuration

The three row configuration was analyzed in order to confirm the findings from the four row configuration concerning the 2D calculation procedure. Fig. 10 shows a comparison between 2D, 3D and quasi-3D calculation results for the overall cooling effectiveness. As it can be seen from this figure, the agreement between the quasi-3D simulations and the 3D calculations is very good. This can be taken as a further confirmation of the previously described procedure for selecting suitable 2D models.

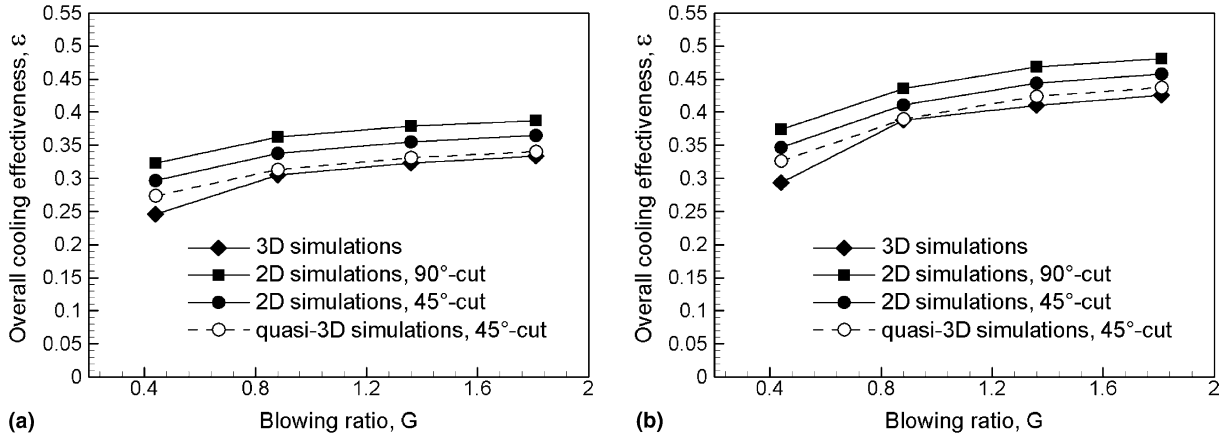

Fig. 9. Comparisons between the 2D, quasi-3D and 3D simulations performed at REC (four-row cylindrical model). (a) Low h_{plen} and (b) high h_{plen}.

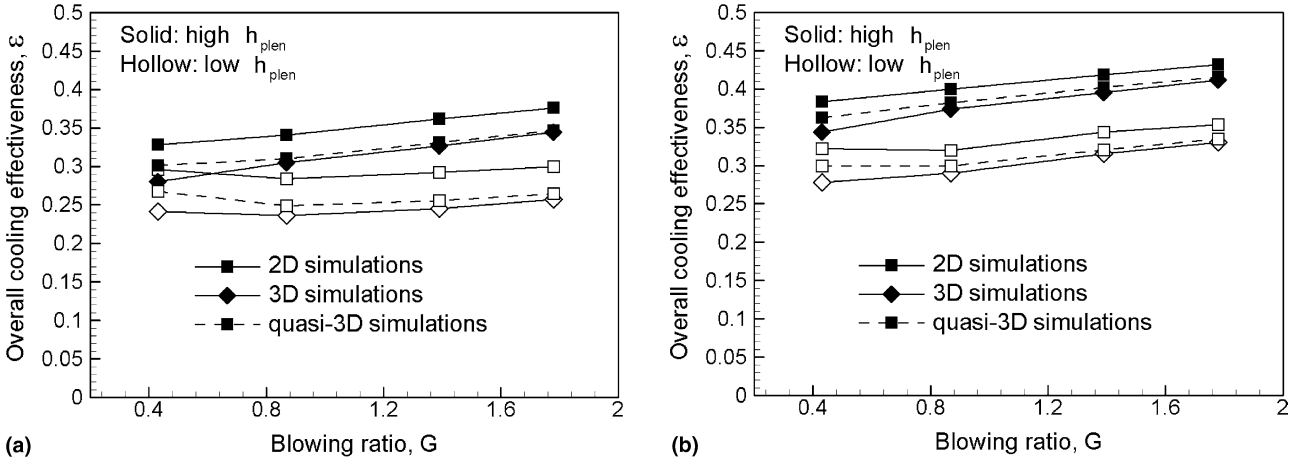

Fig. 10. Comparisons between the 3D, 2D and quasi-3D simulations corresponding to the three row cylindrical model. (a) Real blade material (REC) and (b) low-conductivity material (EPFL conditions).

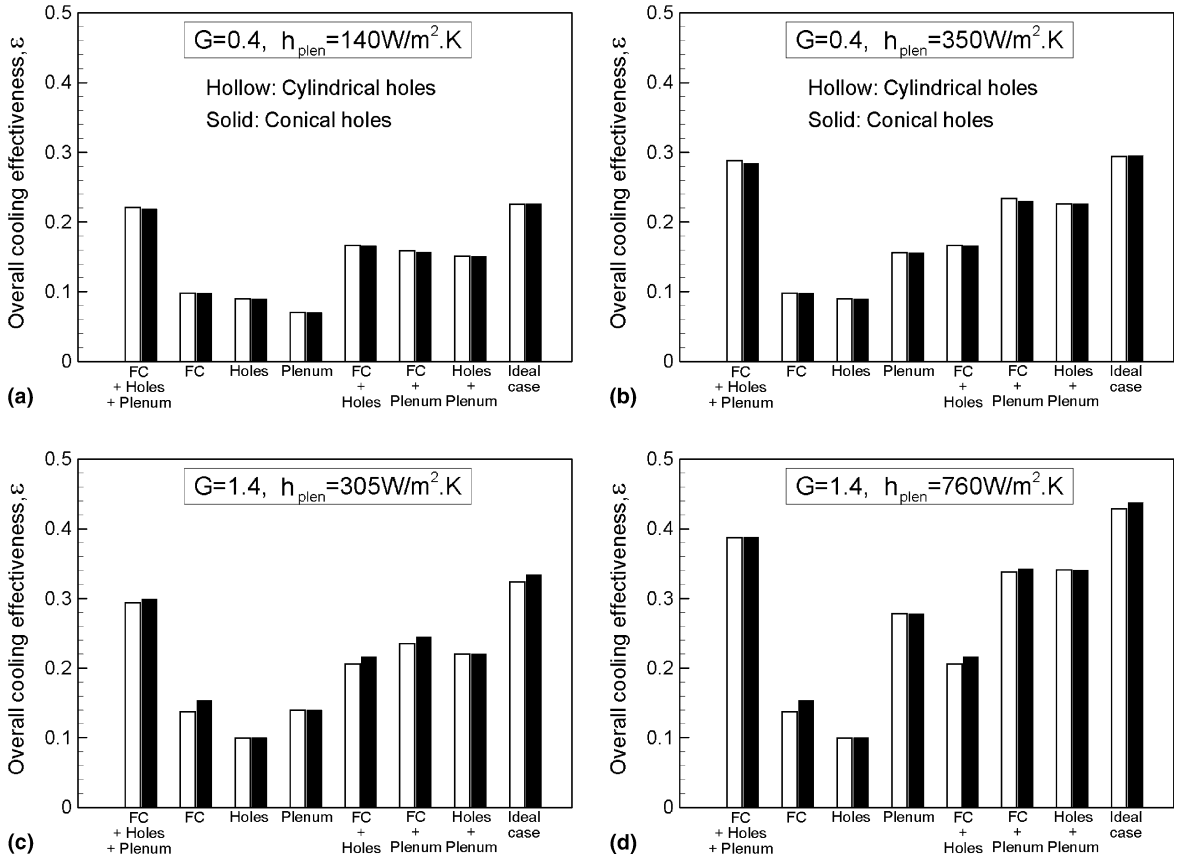

Fig. 11. Contributions of the different cooling mechanisms at REC: 2D finite element calculations for cylindrical and conical holes for the blunt body. (a) Low G, low h_{plen}, (b) low G, high h_{plen}, (c) high G, low h_{plen}, (d) high G, high h_{plen}.

4.2. Numerical results for the blunt body

In order to test the influence of the cooling hole geometry on the showerhead cooling performance, numerical simulations were carried out on two film-cooled blunt bodies. Cylindrical holes were chosen as the reference case. Since the forward-diffused holes offered only a slight film cooling effectiveness enhancement, conical holes were preferred for the follow-on study. Due to the good agreement between the 3D and 2D numerical results found on the cylindrical models, only 2D simulations were carried out on the blunt body models. The influence of the coolant-to-mainstream blowing ratio, the cooling mechanisms associated with film cooling and the thermal conductivity were investigated. Finally, quasi-3D simulations were also carried out to test the influence of the hole number. Computations were performed on a 90°-cut of the 3D model including the four rows of cooling holes. Different blowing ratios, as well as different levels of backside cooling were tested. The heat transfer coefficients inside the plenum chamber (h_{plen}) were evaluated as described in Appendix A. The influence of the three cooling mechanisms was investigated at REC. The numerical simulations were performed on a 90°-cut of the blunt body model. Two injection rates, as well as two levels of backside cooling were tested. The values of the overall cooling effectiveness obtained for the different contributions were compared to those evaluated for the reference cases (original and ideal cases), as described before. The results are depicted in Fig. 11. No significant differences are observed between the cylindrical and conical holes. Nevertheless, at $G = 1.4$, the conical holes provide a mild enhancement of the overall cooling effectiveness, especially for the contributions that include the external film cooling. A comparison with the results obtained for the four-row cylinder configuration (Fig. 7) shows that the effects of all cooling mechanisms are similar. Nevertheless, the comparison also yields that for all test cases, the values of the overall cooling effectiveness are lower on the blunt body models.

5. Conclusions

Based on the numerical calculations carried out in the present investigation, the following major conclusions might be drawn:

- A correct evaluation of a showerhead cooling configuration always needs to take all different cooling mechanisms into account.
- Analyzing the showerhead geometry by 3D finite element models allows to obtain detailed knowledge of the heat transfer process.

- A 2D approach has been presented which can be used to reliably predict the cooling effectiveness of the blade. This approach takes seconds, compared to 3D calculations, which take hours or even days.

Acknowledgements

The LTT kindly acknowledge the financial support of the present project by ALSTOM Power Switzerland. Furthermore, we would like to acknowledge the fruitful discussions with Prof. A. Bölcs (LTT, EPFL), Prof. J. von Wolfersdorf (ITLR, University of Stuttgart) and Dr. S. Parneix (ALSTOM Power Switzerland) concerning various aspects of this project.

Appendix A. Calculation conditions for finite element analysis

Calculation conditions were developed for several solid models, having different material properties and working at varied operating conditions.

A.1. External calculation conditions for 3D calculations

For the experimental boundary conditions (EPFL conditions), the heat transfer coefficients were directly obtained from the liquid crystal measurements. The adiabatic wall temperatures were calculated using:

$$[T_{aw}]_{\text{EPFL conditions}} = [\eta(T_{tc} - T_{tg}) + T_{rg}]_{\text{EPFL conditions}} \quad (A.1)$$

where the film cooling effectiveness η was obtained from the measurements.

For the real engine conditions (REC), the external heat transfer coefficients and adiabatic wall temperatures were calculated from the measurements taking into account the assumption that the Frössling number ($Nu_D/Re_D^{0.5}$), as a similarity parameter, stays constant between the experimental and the engine conditions. The adiabatic wall temperatures were evaluated from the film cooling effectiveness assuming that it was constant between experimental and real engine conditions:

$$[T_{aw}]_{REC} = [\eta]_{\text{EPFL conditions}}[T_{tc} - T_{tg}]_{REC} + [T_{rg}]_{REC} \quad (A.2)$$

A.2. Heat transfer coefficients inside the holes

Empirical correlations were used to calculate heat transfer coefficients inside the cooling holes. Two different cases were distinguished in order to take into account the flow regime, either laminar or turbulent. The flow inside the cylindrical hole was considered laminar for $Re_d \leqslant 3000$ and turbulent for $Re_d > 3000$. For shaped holes, the local hydraulic diameter has been used in the correlations. For a detailed explanation of the used correlations, the reader is referred to [8].

A.3. Temperatures inside the holes

Due to heat exchange occurring inside the cooling holes during the coolant injection, the temperature of the coolant gas changes as it passes through the holes. Consequently, for the numerical calculations, a variation of the coolant temperature was taken into account inside the film holes. Assuming a linear temperature distribution inside the cooling holes and employing a heat balance, the outlet temperature T_o can be calculated according to

$$T_o = \frac{\tilde{h}_c A_h}{\dot{m} c_p}(\widetilde{T}_w - \widetilde{T}_c) + T_i \quad (A.3)$$

where T_i is the inlet temperature in the hole, $\tilde{h}_c$ is the averaged heat transfer coefficient inside the hole. In order to take into account the entrance effects, $\tilde{h}_c$ is the mean heat transfer coefficient for the length under consideration. $\widetilde{T}_c$ is the averaged coolant temperature inside the hole. $\widetilde{T}_w$ is the averaged wall temperature and is unknown. To initialize the first calculation the unknown wall temperature is simply taken as an average value of the hot gas and coolant temperature. For the 2D calculations, the coolant temperatures were evaluated based on Eq. (A.3). For the 3D calculations the coolant temperatures have been iterated from the known temperature field. The reader is referred to [8] for more detailed information on the used procedure.

A.4. Calculation conditions inside the plenum chamber

Empirical correlations were also used to evaluate heat transfer coefficients inside the plenum chamber. The reader is referred to [8] for detailed information on the used correlations. The temperature of the coolant inside the plenum chamber was assumed to be constant and equal to the total temperature.

References

[1] C. Falcoz, B. Weigand, P. Ott, Experimental investigations on showerhead cooling on a blunt body, Int. J. Heat Mass Transfer, in press, doi:10.1016/j.ijheatmasstransfer.2005.10.012.
[2] R.E. Mayle, F.J. Camarata, Heat transfer investigation for multihole aircraft turbine blade cooling, AFAPL-Tr-73-30, 1973.
[3] N. Kasagi, M. Hirata, M. Kumada, Studies of full coverage film cooling, Part 1: Cooling effectiveness of thermally conductive wall, ASME 81-GT-37, 1981.
[4] M. Kumada, M. Hirata, N. Kasagi, Studies of full coverage film cooling, Part 2: Measurements of local heat transfer coefficient. ASME 81-GT-38, 1981.
[5] A.R. Wadia, D.A. Nealy, Development of a design model for airfoil leading edge film cooling. ASME 85-GT-120, 1985.
[6] M. Martiny, A. Schulz, S. Wittig, Mathematical model describing the coupled heat transfer in effusion-cooled combustor walls. ASME 97-GT-329, 1997.
[7] A. Hoffs, U. Drost, A. Bölcs, An investigation of effectiveness and heat transfer on a showerhead-cooled cylinder. ASME 97-GT-069, 1997.
[8] C. Falcoz, A comparative study of showerhead cooling performance. Ph.D. Thesis No. 2735, Swiss Federal Institute of Technology-Lausanne, 2003.

[9] H.S. Carslaw, J.C. Jaeger, Conduction of Heat in Solids, second ed., Oxford Science Publications, 1992.
[10] ABAQUS, Users manual for Version 5.8, Hibbitt Karlsson and Sorensen Inc., Rhode Island, vol. I–III, 1998.
[11] I-DEAS, User's guide, Structural dynamics research corporation, Milford, Ohio, vol. 1, 1996.
[12] S.W. Sloan, A fast algorithm for constructing Delaunay triangulations in the plane, Adv. Eng. Software 9 (1987) 34–54.